

# Real-space computation of $E/B$ -mode maps I: Formalism and Compact Kernels

**Aditya Rotti and Kevin Huffenberger**

Department of Physics, Florida State University, Keen Physics Building, 77 Chieftan Way, Tallahassee, Florida, U.S.A.

E-mail: [adityarotti@gmail.com](mailto:adityarotti@gmail.com), [khuffenberger@fsu.edu](mailto:khuffenberger@fsu.edu)

**Abstract.** We derive full-sky, real-space operators that convert between polarization Stokes  $Q/U$  parameters to the coordinate-independent scalar  $E/B$  modes that are widely used in Cosmic Microwave Background(CMB) and cosmic shear analysis. The convolution kernels split naturally into angular and radial parts and we show explicitly how the radial extent of the convolution kernel depends on the targeted band-limit. We show that an arbitrary radial dependence can produce  $E/B$ -like maps and that these are simply filtered versions of the standard  $E/B$  maps. This allows us to compute  $E/B$  maps in real space with a compactly-supported kernel, an approach that can guarantee the avoidance of known foreground regions and can be employed in a massively parallel scheme at high-resolution. We can recover the standard power spectrum of the polarized CMB sky by correcting the power spectra of these maps with a simple window function. The spatial structure of the real space operator provides great intuition for the  $E/B$  structure of polarized, filamentary galactic foregrounds and we predict non-zero B-mode signature that is expected from finite filaments in the sky. We cast the standard CMB polarization analysis operators in a matrix-vector notation which facilitates the derivations and shows that the kernels relate directly to spin-0  $Y_{\ell 2}$  spherical harmonic functions. This new notation also allows us to derive real space operators which decompose the measured Stokes parameters into their even and odd-parity parts, without ever evaluating the scalar  $E/B$  fields themselves. This paper is the first part in a series of papers that explore real-space computation of polarization modes and their applications.

---

## Contents

<b>1</b>	<b>Introduction</b>	<b>1</b>
<b>2</b>	<b>Polarization primer</b>	<b>2</b>
2.1	A heuristic argument for real space construction of $E/B$ fields on the sphere	2
2.2	Standard $E/B$ fields	4
2.3	Matrix notation	5
<b>3</b>	<b>Real space polarization operators</b>	<b>6</b>
3.1	Evaluating scalar $E/B$ from Stokes $Q/U$	6
3.2	Evaluating Stokes $Q/U$ from scalar $E/B$	9
3.3	Visualizing the real space kernels	10
3.4	Purifying Stokes parameters $Q/U$ for $E/B$ modes	10
3.5	The non-locality of the real space operators	15
3.6	Generalized polarization operators	17
3.6.1	Recovering the standard $E$ and $B$ mode spectra	18
<b>4</b>	<b>Understanding polarization signatures of magnetized filaments</b>	<b>20</b>
<b>5</b>	<b>Discussion</b>	<b>22</b>

---

## 1 Introduction

During recombination, the Cosmic Mircowave Background undergoes Thomson scattering that leaves it with  $\sim 5$  percent linear polarization. The polarization signal contains information about the plasma velocity and provides cosmological constraints independent from the signal in temperature [1]. The standard analysis technique converts the Stokes parameters of polarization into scalar ( $E$ ) and pseudo-scalar ( $B$ ) modes, which are easier to compare to theory. The pseudo-scalar  $B$  mode is particularly important because it cannot be generated by primordial scalar pertubations. Thus any  $B$ -modes that appear must be from: (1) primordial tensor perturbations (gravitational waves), which reveal the energy scale of inflation [2, 3]; (2) lensing of  $E$ -modes, which helps to reveal the distribution of matter in the universe; (3) foregrounds (especially Galactic synchrotron and dust emission) [4]; (4) unknown systematic problems in the data; (5) unknown, exotic phenemena like cosmic birefringence or primordial magnetic fields [5–8].

The formalism for converting the Stokes parameters to scalar quantities is well established [9, 10]. The reason we take a detailed look at it here is that with renewed focus on foreground contamination to the  $B$ -mode signal, we wanted to gain an intuition for what  $E/B$  mode patterns arise from physical polarized structures in the galaxy. We also wanted to gain insight into the problem of masking and the non-locality of the  $E/B$  fields compared to the Stokes parameters.

The spin-0 scalar  $E/B$  modes relate to the spin-2 complex Stokes parameters via the spin-raising and -lowering operators  $(\eth, \bar{\eth})$ , which are second derivatives evaluated locally. However, in practice we compute  $E/B$  modes to a specified band limit, and this makes them

non-local functions of the polarization field. In other words, the  $E/B$  modes at a point can get contributions from all over the sky.

(stuff about foregrounds, masking, ambiguous modes with references)

Zaldarriaga explored the spatial real-space kernels in the flat-sky approximation [11].

This paper is organized in the following manner: In Sec. 2 we present a primer on the description of CMB polarization on the sphere. Here we begin with a heuristic argument that makes transparent the real space construction of E/B modes on the sphere. We discuss the standard harmonic space procedures for this operation. Finally we introduce the matrix-vector notation which yields a more concise description of the harmonic space procedures. In Sec. 3.1 and Sec. 3.2 we derive and discuss the real space operators that transform Q/U to E/B and vice versa. In Sec. 3.3 we evaluate these real space operators and present visualizations of these functions. In Sec. 3.4 we derive a real space operator that decomposes the Stokes Q/U parameters into components that correspond to E and B modes respectively and present its visualizations. In Sec. 3.5 we study the locality of the real space operators and explore its band limit dependence. In Sec. 3.6 we present a systematic way to generalize the real space operators by varying the non-locality parameter and discuss the connection to the spin raising and lower operators. We conclude with a summary and discuss the scope of this new method of analyzing CMB polarization in Sec. 5.

## 2 Polarization primer

### 2.1 A heuristic argument for real space construction of E/B fields on the sphere

CMB polarization is measured in terms of Stokes parameters, time averages of the linear polarization of the electric field along cartesian axes perpendicular to the line of sight.<sup>1</sup> Thus Stokes  $Q$  and  $U$  depend on the choice of the local coordinate system and a rotation by an angle  $\psi$  around the line of sight transforms them as:

$$\begin{bmatrix} Q \\ U \end{bmatrix}' = \begin{bmatrix} \cos 2\psi & \sin 2\psi \\ -\sin 2\psi & \cos 2\psi \end{bmatrix} \begin{bmatrix} Q \\ U \end{bmatrix}. \quad (2.1)$$

Equivalently the object  $\pm_2 \bar{X}(\hat{n}) = Q(\hat{n}) \pm iU(\hat{n})$  transforms as  $\pm_2 f' = e^{\mp 2i\psi} s f$  and hence forms a spin-2 field [12].

The standard construction of  $E$  and  $B$  fields arise from the desire to have a coordinate independent description of the polarization. This follows from operations that raise (or lower) the spin of the  $X$  field to construct scalar fields. But from the transform properties of the Stokes parameters, we can already construct a heuristic argument for what these operations must look like in real space.

We consider the contribution to a scalar field at  $\hat{n}_e$  from the polarization field at  $\hat{n}_q$ . Fig. 1 shows that the transformation of the local coordinate system between the two positions can be described by a counter-clockwise rotation around the local  $\hat{n}_q$  (unit outward pointing radial vector at  $(\theta_q, \phi_q)$ ) by angle  $\alpha$ , parallel transport by angle  $\beta$  along the shorter geodesic and a counter-clockwise rotation around  $\hat{n}_q$  by  $-\gamma$ . This corresponds to a rotation by Euler angles  $(\alpha, \beta, -\gamma)$  in the  $z - y_1 - z_2$  convention.<sup>2</sup>

---

<sup>1</sup>Throughout we use the conventions of HEALPix [?], measuring the polarization angle East of South.

<sup>2</sup>The Euler angles in the more standard  $z - y - z$  convention are related to those in the  $z - y_1 - z_2$  convention by the following rule:  $(\alpha, \beta, \gamma)_{z-y-z} = (\gamma, \beta, \alpha)_{z-y_1-z_2}$  [13].

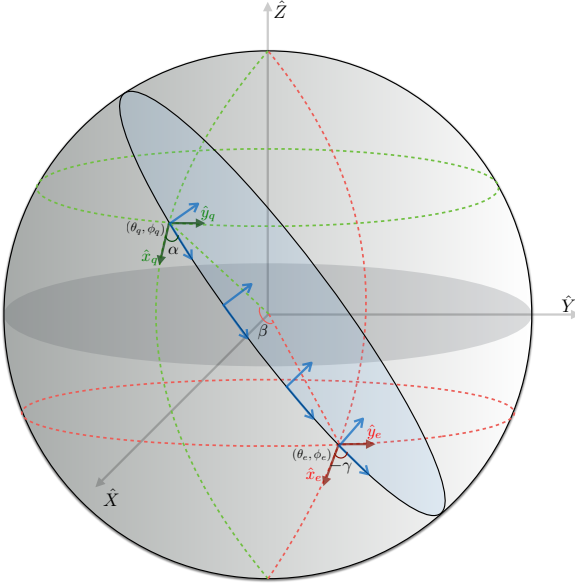


**Figure 1:** This figure depicts the Euler angles in the z-y1-z2 convention. The cartesian coordinates shown in **dark solid green** are those that lie in the tangent plane at location  $\hat{n}_q = (\theta_q, \phi_q)$  while those shown in **dark solid red** are the ones that lie in the tangent plane at location  $\hat{n}_e = (\theta_e, \phi_e)$ . The blue coordinates at different locations are representative of the parallel transport along the geodesic connection the two locations  $\hat{n}_q$  &  $\hat{n}_e$  on the sphere.

Rotating the cartesian coordinates in the tangent plane at location  $\hat{n}_q$  by an angle  $\psi$  about the local  $\hat{z}_q$  axis, the Stokes parameters in the new coordinate system relate to those in the original coordinate system as:  $\mathcal{R}_{\hat{z}_q}(\psi)[{}_{+2}X(\hat{n}_q)] = {}_{+2}X(\hat{n}_q)e^{-i2\psi}$ . This same rotation by  $\psi$  alters the Euler angle  $\alpha_{qe}$  (that aligns the  $x$ -axis at  $\hat{n}_q$  along the geodesic to the location  $\hat{n}_e$ ):  $\mathcal{R}_{\hat{z}_q}(\psi)[\alpha_{qe}] = \alpha_{qe} - \psi$ . Therefore one can see that  $\mathcal{R}_{\hat{z}_q}(\psi)[e^{-i2\alpha_{qe}}] = e^{-i2\alpha_{qe}}e^{i2\psi}$ .

Given these transformation properties, the combination  ${}_{+2}X(\hat{n}_q)e^{-i2\alpha_{qe}}$  is invariant under rotations and must be spin-0 by definition:

$$\mathcal{R}_{\hat{z}_q}(\psi)[{}_{+2}X(\hat{n}_q)e^{-i2\alpha'_{qe}}] = {}_{+2}X(\hat{n}_q)e^{-i2\alpha_{qe}}. \quad (2.2)$$

Further note that  $Q$  &  $\cos 2\alpha$  have even parity since they do not change sign when  $\hat{x} \rightarrow -\hat{x}$  (or  $\hat{y} \rightarrow -\hat{y}$ ) while  $U$  &  $\sin 2\alpha$  change sign under this transformation and hence have odd parity. The real part of the function  ${}_{+2}X(\hat{n}_q)e^{-i2\alpha_{qe}}$  is composed of  $Q \cos 2\alpha$  &  $U \sin 2\alpha$  which are product of functions having the same parity and hence the real part must have even parity. Similarly the imaginary part of the function is composed of  $Q \sin 2\alpha$  &  $U \cos 2\alpha$  which are product of functions having opposite parity and hence the imaginary part must have an odd parity. Therefore we can make the association that contributions to  $(E + iB)(\hat{n}_e)$  must be proportional to  ${}_{+2}X(\hat{n}_q)e^{-i2\alpha_{qe}}$ .

The same rotation  $\mathcal{R}_{\hat{z}_q}(\psi)$  leaves the Euler angle  $|\beta_{qe}|$  unaltered (it measures the angular distance between the points). Thus we can conclude that the contribution to  $(E + iB)(\hat{n}_e)$  from the position  $n_q$  must have the form:

$${}_{+2}X(\hat{n}_q)f(\beta_{qe})e^{-i2\alpha_{qe}} \quad (2.3)$$

for some real function  $f$ . Note that when the two locations coincide ( $\beta_{qe} = 0$ ) then  $\alpha_{qe} = 0, 2\pi, 4\pi, \dots$ , implying  $E + iB \propto Q + iU$ . This is a contradiction because  $Q + iU$  does

not transform as a spin-0 field under local rotations, and so we must have  $f(\beta_{qe} = 0) = 0$ . Hence the  $E/B$  fields are necessarily non-local. A similar contradiction arises when the two locations are diametrically opposite,  $\beta_{qe} = \pi$ , and so  $f(\beta_{qe} = \pi) = 0$ . Any such function  $f$  will let us construct  $E/B$ -like scalar fields. Below we derive the particular one that gives rise to our familiar  $E/B$  modes.

This type of real-space construction can be generalized to transform a field of any spin to a field of any other spin, not just two and zero, and so we can use a similar construction (in the opposite direction) to transform  $E/B$  maps back to the Stokes parameters (i.e. transforming spin-0 fields to spin-2).

## 2.2 Standard $E/B$ fields

The standard construction of  $E/B$  fields depend on the spin-raising and -lowering operators, and is usually carried out in harmonic space. The spin-raising operator ( $\eth$ ), applied to a field of spin- $s$   ${}_s g$ , results in a field with spin- $(s+1)$ :  $(\eth_s g)' = e^{-i(s+1)\psi}(\eth_s g)$  [14]. The complementary spin-lowering operator ( $\bar{\eth}$ ) similarly results in a field with spin- $(s-1)$ :  $(\bar{\eth}_s g)' = e^{-i(s-1)\psi}(\bar{\eth}_s g)$ . The complex spin-0 scalar now arise from the spin-2 fields  ${}_{\pm 2} X$  as follows,

$$\mathcal{E}(\hat{n}) + i\mathcal{B}(\hat{n}) = -\bar{\eth}_{+2}^2 \bar{X}(\hat{n}), \quad (2.4a)$$

$$\mathcal{E}(\hat{n}) - i\mathcal{B}(\hat{n}) = -\eth_{-2}^2 \bar{X}(\hat{n}). \quad (2.4b)$$

The  $\mathcal{E}/\mathcal{B}$  fields are defined locally at point  $\hat{n}$  in terms of the operators  $\eth$  and  $\bar{\eth}$ .

It is possible to decompose the complex field  ${}_{\pm 2} \bar{X}$  into spin spherical harmonic functions:  ${}_{\pm 2} \bar{X}(\hat{n}) = \sum_{\ell m} {}_{\pm 2} X_{\ell m} {}_{\pm 2} Y_{\ell m}(\hat{n})$ . Applying the spin raising and lowering operators on the spin spherical harmonic functions leads to the following identities [14]:

$$\eth_s Y_{\ell m}(\hat{n}) = \sqrt{(\ell-s)(\ell+s+1)} {}_{s+1} Y_{\ell m}(\hat{n}), \quad (2.5a)$$

$$\bar{\eth}_s Y_{\ell m}(\hat{n}) = -\sqrt{(\ell+s)(\ell-s+1)} {}_{s-1} Y_{\ell m}(\hat{n}), \quad (2.5b)$$

where  ${}_s Y_{\ell m}(\hat{n})$  denote the spin- $s$  spherical harmonics.

From the definition of  $\mathcal{E}/\mathcal{B}$ , the spin spherical harmonic decomposition of  ${}_{\pm 2} \bar{X}$ , and the identities given in Eq. (2.5), it follows that the scalar fields  $\mathcal{E}/\mathcal{B}$  are given by the equations:

$$\mathcal{E}(\hat{n}) = \sum_{\ell m} a_{\ell m}^E \sqrt{\frac{(\ell+2)!}{(\ell-2)!}} Y_{\ell m}(\hat{n}) \quad ; \quad \mathcal{B}(\hat{n}) = \sum_{\ell m} a_{\ell m}^B \sqrt{\frac{(\ell+2)!}{(\ell-2)!}} Y_{\ell m}(\hat{n}), \quad (2.6)$$

where the harmonic coefficients  $a_{\ell m}^E$  and  $a_{\ell m}^B$  relate to the harmonic coefficients of the spin-2 polarization field via the following equations:

$$a_{\ell m}^E = -\frac{1}{2} \left[ {}_{+2} \tilde{X}_{\ell m} + {}_{-2} \tilde{X}_{\ell m} \right] \quad ; \quad a_{\ell m}^B = -\frac{1}{2i} \left[ {}_{+2} \tilde{X}_{\ell m} - {}_{-2} \tilde{X}_{\ell m} \right]. \quad (2.7)$$

In the remainder of this article, we will work with the scalar  $E$  and pseudo scalar  $B$  fields, defined by:

$$E(\hat{n}) = \sum_{\ell m} a_{\ell m}^E Y_{\ell m}(\hat{n}) \quad ; \quad B(\hat{n}) = \sum_{\ell m} a_{\ell m}^B Y_{\ell m}(\hat{n}). \quad (2.8)$$

These  $E/B$  fields are merely red-filtered  $\Rightarrow$  Is this unambiguously understood as down weighing the high multipoles? versions of  $\mathcal{E}/\mathcal{B}$  (their spherical harmonic coefficients of expansion are related by the factor  $[(\ell+2)!/(\ell-2)!]^{1/2}$ ) and are not local functions of Stokes  $Q/U$ .

### 2.3 Matrix notation

Our derivation of real space operators is more transparent in a matrix-vector notation.<sup>3</sup> We introduce a matrix that encodes spin spherical harmonic basis vectors:

$$|s|\mathcal{Y} = \begin{bmatrix} {}^{+s}Y & 0 \\ 0 & {}^{-s}Y \end{bmatrix}_{2N_{\text{pix}} \times 2N_{\text{alms}}} ; \quad |s|\mathcal{Y}^\dagger = \Delta\Omega \begin{bmatrix} {}^{+s}Y^\dagger & 0 \\ 0 & {}^{-s}Y^\dagger \end{bmatrix}_{2N_{\text{alms}} \times 2N_{\text{pix}}} , \quad (2.9)$$

where  $s$  denotes the spin of the basis functions and our definition of  $|s|\mathcal{Y}^\dagger$  differs from the conventional dagger operation by the factor  $\Delta\Omega$  which is introduced to ensure the ortho-normality of the basis functions:  $|s|\mathcal{Y}^\dagger|s|\mathcal{Y} = I_{2N_{\text{alms}} \times 2N_{\text{alms}}}$  on the discretized sphere.

We will be working with cases  $s \in [0, 2]$ . Each column of  $|s|\mathcal{Y}$  maps to a specific harmonic basis function (i.e. indexed by  $\ell m$ ) and each row maps to a pixel on the sphere. This matrix is not square in general: the number of rows is determined by the pixelization and the number of columns is set by the number of basis functions (e.g. determined by the band limit).

We now define the different polarization data vectors and their representation in real and harmonic space as follows<sup>4</sup>:

$$\bar{S} = \begin{bmatrix} E \\ B \end{bmatrix}_{2N_{\text{pix}} \times 1} ; \quad \bar{X} = \begin{bmatrix} {}^{+2}X \\ {}^{-2}X \end{bmatrix}_{2N_{\text{pix}} \times 1} ; \quad \bar{P} = \begin{bmatrix} Q \\ U \end{bmatrix}_{2N_{\text{pix}} \times 1} , \quad (2.10a)$$

$$\tilde{S} = \begin{bmatrix} a^E \\ a^B \end{bmatrix}_{2N_{\text{alms}} \times 1} ; \quad \tilde{X} = \begin{bmatrix} {}^{+2}\tilde{X} \\ {}^{-2}\tilde{X} \end{bmatrix}_{2N_{\text{alms}} \times 1} . \quad (2.10b)$$

The different symbols have the same meaning as that discussed in Sec. 2, except that the subscript  $\ell m$  for the spherical harmonic coefficients is suppressed for cleaner notation.

We define transformations between different representations of the polarization field (i.e. from  $Q, U$  to  $\pm_2 \bar{X}$  and back):

$$\bar{T} = \begin{bmatrix} 1 & i\mathbb{1} \\ 1 & -i\mathbb{1} \end{bmatrix}_{2N_{\text{pix}} \times 2N_{\text{pix}}} ; \quad \bar{T}^{-1} = \frac{1}{2}\bar{T}^\dagger , \quad (2.11a)$$

$$\tilde{T} = -\begin{bmatrix} 1 & i\mathbb{1} \\ 1 & -i\mathbb{1} \end{bmatrix}_{2N_{\text{alms}} \times 2N_{\text{alms}}} ; \quad \tilde{T}^{-1} = \frac{1}{2}\tilde{T}^\dagger , \quad (2.11b)$$

The sign conventions we have chosen match HEALPix. Using the data vectors and the matrix operators defined above we can now express, in compact notation, the forward and inverse relations between different representations of the polarization data vectors via the following equations:

$$\bar{X} = \bar{T}\bar{P} \quad ; \quad \bar{P} = \frac{1}{2}\bar{T}^\dagger\bar{X} , \quad (2.12a)$$

$$\tilde{X} = \tilde{T}\tilde{S} \quad ; \quad \tilde{S} = \frac{1}{2}\tilde{T}^\dagger\tilde{X} . \quad (2.12b)$$

Meanwhile the spherical harmonic transforms are written as:

$$\bar{X} = {}_2\mathcal{Y}\tilde{X} ; \quad \tilde{X} = {}_2\mathcal{Y}^\dagger\bar{X} ; \quad (2.12c)$$

$$\bar{S} = {}_0\mathcal{Y}\tilde{S} ; \quad \tilde{S} = {}_0\mathcal{Y}^\dagger\bar{S} . \quad (2.12d)$$

---

<sup>3</sup>While we work with the matrix and vector sizes given in terms of some pixelization parameter  $N_{\text{pix}}$ , all the relations are equally valid in the continuum limit attained by allowing  $N_{\text{pix}} \rightarrow \infty$

<sup>4</sup>We adopt a convention in which real space quantities are denoted by bar-ed variable while those in harmonic space are denoted by tilde-ed variables, as in [11].

Finally we introduce the operators that project harmonic space data vector to the  $E$  or  $B$  subspace:

$$\tilde{O}_E = \begin{bmatrix} \mathbb{1} & 0 \\ 0 & 0 \end{bmatrix}_{2N_{\text{alms}} \times 2N_{\text{alms}}} ; \quad \tilde{S}_E = \tilde{O}_E \tilde{S}, \quad (2.13a)$$

$$\tilde{O}_B = \begin{bmatrix} 0 & 0 \\ 0 & \mathbb{1} \end{bmatrix}_{2N_{\text{alms}} \times 2N_{\text{alms}}} ; \quad \tilde{S}_B = \tilde{O}_B \tilde{S}. \quad (2.13b)$$

Note that these harmonic space matrices are idempotent: ( $\tilde{O}_E \tilde{O}_E = \tilde{O}_E$ ;  $\tilde{O}_B \tilde{O}_B = \tilde{O}_B$ ), orthogonal: ( $\tilde{O}_E \tilde{O}_B = \mathbb{0}$ ), and sum to the identity matrix: ( $\tilde{O}_E + \tilde{O}_B = \mathbb{1}$ ). The above relations for these harmonic space operators are exactly valid. In the following sections we derive the real space analogues ( $O_E, O_B$ ) of these harmonic space operators.

### 3 Real space polarization operators

#### 3.1 Evaluating scalar $E/B$ from Stokes $Q/U$

In Sec. 2 we described the conventional procedure of computing the scalar fields  $E/B$  from the Stokes parameters  $Q/U$ . In this section we derive the real space convolution kernels on the sphere which can be used to directly evaluate the scalar fields  $E$  &  $B$  on the sphere. We use the vector-matrix notation introduced in Sec. 2.3 to write down an operator equation relating the real space vector of scalars  $\bar{S}$  to the Stokes polarization vector  $\bar{P}$ :

$$\bar{S} = {}_0\mathcal{Y} \tilde{T}^{-1} {}_2\mathcal{Y}^\dagger \bar{T} \bar{P} = \frac{1}{2} {}_0\mathcal{Y} \tilde{T}^\dagger {}_2\mathcal{Y}^\dagger \bar{T} \bar{P}, \quad (3.1a)$$

$$= \bar{O} \bar{P}. \quad (3.1b)$$

The explicit form of the real space operator  $\bar{O}$  can be derived by contracting over all the matrix operators. This procedure is explicitly worked out in the following set of equations:

$$\bar{O} = \frac{1}{2} {}_0\mathcal{Y} \tilde{T}^\dagger {}_2\mathcal{Y}^\dagger \bar{T}, \quad (3.2a)$$

$$= -0.5\Delta\Omega \begin{bmatrix} {}_0Y_e & 0 \\ 0 & {}_0Y_e \end{bmatrix} \begin{bmatrix} \mathbb{1} & \mathbb{1} \\ -i\mathbb{1} & i\mathbb{1} \end{bmatrix} \begin{bmatrix} {}_{+2}Y_q^\dagger & 0 \\ 0 & {}_{-2}Y_q^\dagger \end{bmatrix} \begin{bmatrix} \mathbb{1} & i\mathbb{1} \\ \mathbb{1} & -i\mathbb{1} \end{bmatrix}, \quad (3.2b)$$

$$= -0.5\Delta\Omega \begin{bmatrix} \sum({}_0Y_e {}_2Y_q^\dagger + {}_0Y_e {}_{-2}Y_q^\dagger) & i\sum({}_0Y_e {}_2Y_q^\dagger - {}_0Y_e {}_{-2}Y_q^\dagger) \\ -i\sum({}_0Y_e {}_2Y_q^\dagger - {}_0Y_e {}_{-2}Y_q^\dagger) & \sum({}_0Y_e {}_2Y_q^\dagger + {}_0Y_e {}_{-2}Y_q^\dagger) \end{bmatrix}, \quad (3.2c)$$

where the symbol  ${}_0Y_e$  is used to denote the sub-matrix  ${}_{0\hat{n}_e \times \ell m} Y_{\ell m} \equiv {}_0Y_{\ell m}(\hat{n}_e)$ , the symbol  ${}_{\pm 2}Y_q^\dagger$  is used to denote the transposed conjugated matrix  ${}_{\pm 2}Y_{\ell m \times \hat{n}_q}^* \equiv {}_{\pm 2}Y_{\ell m}^*(\hat{n}_q)$  and the summation is over the multipole indices  $\ell, m$ . As before, we use the notation that the index  $e$  denotes the location where the scalar fields are being evaluated, and the index  $q$  denotes the location from which the Stokes parameters are being accessed. Using the conjugation properties of the spin spherical harmonic functions it can be shown that the following identity holds true:

$$\left[ \sum_{\ell m} {}_0Y_{\ell m}(\hat{n}_e) {}_{+2}Y_{\ell m}^*(\hat{n}_q) \right]^* = \sum_{\ell m} {}_0Y_{\ell m}(\hat{n}_e) {}_{-2}Y_{\ell m}^*(\hat{n}_q), \quad (3.3)$$

where the terms on either side of the equation are those that appear in Eq. (3.2c). Note that the operator  $\bar{O}$  is real as one expects, since each sub-matrix in Eq. (3.2c) is formed by summing a complex number and its conjugate.

Eq. (3.2c) already presents a real space operator, but it is not in a form which can be practically implemented. To proceed, we use the fact that the  $m$  sum over the product of two spin spherical harmonic functions can be expressed as a function of the Euler angles [13]:

$$\sum_m s_1 Y_{\ell m}^*(\hat{n}_i) s_2 Y_{\ell m}(\hat{n}_j) = \sqrt{\frac{2\ell+1}{4\pi}} s_2 Y_{\ell-s_1}(\beta_{ij}, \alpha_{ij}) e^{-is_2\gamma_{ij}}, \quad (3.4)$$

where  $\alpha_{ij}$ ,  $\beta_{ij}$  &  $\gamma_{ij}$  denote the Euler angles that specifically transform ( $i \rightarrow j$ ): the coordinate system at  $\hat{n}_i$  to align the coordinate system at  $\hat{n}_j$ <sup>5</sup>. Using this identity, the different parts of the real space operator  $\bar{O}$  (from eq. 3.2c) are completely specified by the following complex function:

$$\begin{aligned} \mathcal{M}(\hat{n}_e, \hat{n}_q) &= \mathcal{M}_r + i\mathcal{M}_i, \\ &= \sum_{\ell m} {}_0Y_{\ell m}(\hat{n}_e) {}_{-2}Y_{\ell m}^*(\hat{n}_q) = \sum_{\ell} \sqrt{\frac{2\ell+1}{4\pi}} {}_0Y_{\ell 2}(\beta_{qe}, \alpha_{qe}), \end{aligned} \quad (3.5a)$$

$$= [\cos(2\alpha_{qe}) + i \sin(2\alpha_{qe})] \sum_{\ell=\ell_{\min}}^{\ell_{\max}} \frac{2\ell+1}{4\pi} \sqrt{\frac{(\ell-2)!}{(\ell+2)!}} P_{\ell}^2(\cos \beta_{qe}), \quad (3.5b)$$

$$\mathcal{M}(\beta_{qe}, \alpha_{qe}) = [\cos(2\alpha_{qe}) + i \sin(2\alpha_{qe})] \mathcal{M}f(\beta_{qe}, \ell_{\min}, \ell_{\max}), \quad (3.5c)$$

where we have used the identity in Eq. (3.4) to simplify the product of the spherical harmonic functions. Note that the function depends only on two out of the three Euler angles. The azimuthal part depends only on the Euler angle  $\alpha_{qe}$ , and so its harmonic transform has no multipole  $\ell$  dependence. The azimuthal part is the crucial operation that translates between different spin representation of CMB polarization. Only the radial part  $f(\beta_{qe})$  depends only on the angular separation between locations and hence completely incorporates all the multipole  $\ell$  dependence. Recall that we had guessed the general form of the kernel using simple heuristic arguments in Sec. 2.1. Here we have rigorously derived the exact form of the function  $f(\beta)$ . Studying the  $P_{\ell}^2$  functions in the limits  $\beta \rightarrow 0, \pi$  it is easy to show that  $f(\beta)$  vanishes at  $\beta = 0, \pi$ , as was argued to be a necessary property to yield a field of requisite spin.

Employing Eq. (3.5) to simplify the product of spherical harmonic functions in Eq. (3.2c), the real space operator  $\bar{O}$  can now be cast in this more useful form:

$$\bar{O} = -\Delta\Omega \begin{bmatrix} \mathcal{M}_r & \mathcal{M}_i \\ -\mathcal{M}_i & \mathcal{M}_r \end{bmatrix} = -\Delta\Omega \mathcal{M}f(\beta_{qe}, \ell_{\min}, \ell_{\max}) \begin{bmatrix} \cos(2\alpha_{qe}) & \sin(2\alpha_{qe}) \\ -\sin(2\alpha_{qe}) & \cos(2\alpha_{qe}) \end{bmatrix}, \quad (3.6)$$

where  $(\alpha_{qe}, \beta_{qe}, \gamma_{qe})$  denote the Euler angles which rotate the local cartesian system at  $\hat{n}_q$  (location where Stokes parameters are accessed) to the cartesian system at  $\hat{n}_e$  (location where the scalar fields are evaluated).

---

<sup>5</sup>The sense of the rotation becomes more obvious when this equation is written in terms of the Wigner-D functions.

**Radiation kernel.** The expression we call the *radiation kernel* allows us, like a Green’s function, to evaluate the  $E/B$  field contribution due to a single Stoke parameter “charge” at a fixed location. The total  $E/B$  maps can then be thought of as the superposed radiation emerging from Stokes charges across the sphere. In this picture, we are effectively in the frame of the Stokes charge  $\pm_2 X$  and evaluate its contribution to the complex spin-0 scalar field  $E + iB$  across the sphere. **This one to many mapping from a point in the spin-2 Stokes field to the complex spin-0 (scalar) field across the sphere is graphically represented in Fig. 2.**

The  $E/B$  contribution from the Stokes parameters at some location  $\hat{n}_q$  is given by the following expression (Eq. (3.6) and Eq. (3.1b)):

$$\bar{S}_q(\hat{n}_e) = \begin{bmatrix} E_e \\ B_e \end{bmatrix}_q = -\mathcal{M}f(\beta_{qe}, \ell_{\min}, \ell_{\max}) \begin{bmatrix} \cos(2\alpha_{qe}) & \sin(2\alpha_{qe}) \\ -\sin(2\alpha_{qe}) & \cos(2\alpha_{qe}) \end{bmatrix} \begin{bmatrix} Q_q \\ U_q \end{bmatrix} \Delta\Omega. \quad (3.7)$$

The total map can be simply evaluated by summing over the contribution from the Stokes parameters at each location  $\hat{n}_q$ :  $\bar{S} = \sum_{q=1}^{N_{\text{pix}}} \bar{S}_q$ . This operation can be cast concisely as:

$$[E + iB](\hat{n}_e) = -\Delta\Omega \sum_{q=1}^{N_{\text{pix}}} \left[ {}_{+2}X(\hat{n}_q) e^{-i2\alpha_{qe}} \right] \mathcal{M}f(\beta_{qe}), \quad (3.8a)$$

$$= \sum_{q=1}^{N_{\text{pix}}} {}_{+2}X(\hat{n}_q) \mathcal{M}_G(\hat{n}_e, \hat{n}_q), \quad (3.8b)$$

where  $\Delta\Omega$  denotes the pixel area and the last line is a simple scalar multiplication between complex numbers. The radiation kernel is then:  $\mathcal{M}_G = -\Delta\Omega \mathcal{M}(\beta_{qe}, \alpha_{qe})^*$  which can be thought of as the Green’s function of the operator, since  $[E + iB](\hat{n}_e) = \mathcal{M}_G(\hat{n}_e, \hat{n}_q)$  is the spin-0 scalar field generated from the delta-function Stokes field  $[Q + iU](\hat{n}) = [\delta(\hat{n} - \hat{n}_q) + i0]$ . We display the kernel later in Fig. 3.

**Convolution kernel.** We can also formulate the real space operator as a convolution operation, where the scalar field at  $\hat{n}_e$  gathers contributions from the Stokes fields. This is based around the inverse rotation from the previous section (to align the coordinate system at  $\hat{n}_e$  with that at  $\hat{n}_q$ ). The inverse rotation Euler angles relates to the forward rotation Euler angles by the following relations:  $\alpha_{eq} = -\gamma_{qe}$ ,  $\beta_{eq} = -\beta_{qe}$  and  $\gamma_{eq} = -\alpha_{qe}$ . Since the kernel only depends on the cosine of the Euler angle  $\beta$ , it is immune to changes in its sign. The operator equation can be expressed as a function of the Euler angle  $\gamma_{eq}$  as follows:

$$\begin{bmatrix} E_e \\ B_e \end{bmatrix} = -\Delta\Omega \sum_{q=1}^{N_{\text{pix}}} \mathcal{M}f(\beta_{eq}, \ell_{\min}, \ell_{\max}) \begin{bmatrix} \cos(2\gamma_{eq}) & -\sin(2\gamma_{eq}) \\ \sin(2\gamma_{eq}) & \cos(2\gamma_{eq}) \end{bmatrix} \begin{bmatrix} Q_q \\ U_q \end{bmatrix}, \quad (3.9)$$

This formulation of the real space operator can be interpreted as integrating at some fixed location  $\hat{n}_e$  the  $E/B$  mode contribution arising from the Stokes parameters at all location  $\hat{n}_q$  on the sphere. This operation can be expressed more concisely as follows:

$$[E + iB](\hat{n}_e) = -\Delta\Omega \sum_{q=1}^{N_{\text{pix}}} \mathcal{M}f(\beta_{eq}, \ell_{\min}, \ell_{\max}) \left( e^{i2\gamma_{eq}} {}_{+2}X(\hat{n}_q) \right), \quad (3.10a)$$

$$= \left\{ \mathcal{M}_B \star {}_{+2}X \right\}(\hat{n}_e), \quad (3.10b)$$



**Figure 2:** The local cartesian coordinates  $(\hat{x}, \hat{y})$  are drawn on the red circle(sphere), representative of the coordinate dependence of the Stokes parameters. The two sets of dotted lines drawn at representative points denote great circles, one which passes through the central point labelled ‘e’ and the other chosen such that the two have locally orthogonal tangent vectors  $(\hat{r}, \hat{\phi})$ . The angle  $\alpha_{qe}$  defines a rotation operator that aligns the local  $\hat{x}$  with  $\hat{r}$ . *Convolution kernel:* The resultant scalar field at ‘e’ can be evaluated by summing over the contribution from all the Stokes parameters on the red circle. This convolution is performed with kernels which are defined in term of the Euler angle  $\gamma_{eq}$ . *Radiation kernel:* It is also possible to compute the contribution from the Stokes parameter at ‘q’ to all the point on the blue circle and this is a function of the Euler angle  $\alpha_{qe}$ . On the flat sky  $\gamma_{eq} = -\alpha_{qe}$  and consequently there is no difference between the radiation and convolution kernels.

where  $\star$  denotes a convolution and  $\mathcal{M}_B = -\Delta\Omega\mathcal{M}(\beta_{eq}, \gamma_{eq})$ . When  $\mathcal{M}$  is expressed as a function of the Euler angle  $\gamma_{eq}$  it can be thought of as an effective instrument beam pointing to the direction  $\hat{n}_e$ . This many to one mapping from the spin-2 Stokes field on the sphere to the complex spin-0 (scalar) field at a point on the sphere is graphically represented in Fig. 2. We display the kernel in Fig. 3.

### 3.2 Evaluating Stokes $Q/U$ from scalar $E/B$

The real space operator which translates  $E$  &  $B$  fields to Stokes parameters  $Q$  &  $U$  can be derived using a similar procedure. Expressed in the matrix-vector notation, inverse operator is given by the following equation:

$$\bar{P} = \bar{T}^{-1} {}_2\mathcal{Y}\tilde{T}_0\mathcal{Y}^\dagger \bar{S} = \frac{1}{2}\bar{T}^\dagger {}_2\mathcal{Y}\tilde{T}_0\mathcal{Y}^\dagger \bar{S}, \quad (3.11a)$$

$$= \bar{O}^{-1} \bar{S}. \quad (3.11b)$$

The inverse operator expressed in terms of the function  $\mathcal{M}$  given in Eq. (3.5) is given by the following equation:

$$\bar{O}^{-1} = -\Delta\Omega \begin{bmatrix} \mathcal{M}_r & -\mathcal{M}_i \\ \mathcal{M}_i & \mathcal{M}_r \end{bmatrix} = -\Delta\Omega \mathcal{M}f(\beta_{eq}, \ell_{\min}, \ell_{\max}) \begin{bmatrix} \cos(2\alpha_{qe}) & -\sin(2\alpha_{qe}) \\ \sin(2\alpha_{qe}) & \cos(2\alpha_{qe}) \end{bmatrix}, \quad (3.12)$$

where all the symbols have the same meaning as discussed in Sec. 3.1. Note that the kernel in the above equation differs from the one in Eq. (3.6) by a change in sign on the off-diagonals

of the block matrix. When expressed in terms of the same set of Euler angles used to define the operator  $\bar{O}$ , it can be shown that the different forms of the real space operator are given by the following equations:

$${}_{+2}X(\hat{n}_q) = \sum_{e=1}^{N_{\text{pix}}} [E + iB](\hat{n}_e) \mathcal{M}_B^*(\hat{n}_e) \quad \text{Radiation kernel ,} \quad (3.13)$$

$${}_{+2}X(\hat{n}_q) = \left\{ \mathcal{M}_G^* \star [E + iB] \right\}(\hat{n}_q) \quad \text{Convolution kernel ,} \quad (3.14)$$

where all the symbols have the same meaning as defined in Sec. 3.1. Note that the conjugated forms of the Green's function and the effective beam for the operator  $\bar{O}$  have their roles reversed for the inverse operator  $\bar{O}^{-1}$ .

### 3.3 Visualizing the real space kernels

We compute the Euler angles  $(\alpha, \beta, \gamma)$  given the angular coordinates of any two Healpix pixels and use these to evaluate the convolution and radiation kernels. To provide an intuition for how these kernels vary as a function of position of the central pixel we depict in Fig. 3 the respective kernels at a few different locations on the sphere. While the kernels are evaluated in the band limit  $\ell \in [2, 192]$ , for illustration these functions are sampled at a very high Healpix resolution parameter of NSIDE=2048. All the plots have been rotated such that the central location marked by the black circle are in the centre of the figure. The horizontal and vertical lines that pass through the central black circle mark the local latitude and longitude respectively.

The real and imaginary part of the kernel  $\mathcal{M}_G$  are identical irrespective of changes in the galactic latitude and longitude of the central pixel. These functions are not distorted when a part of the domain overlaps with the poles, as can be seen in the first two rows of Fig. 3. These observations are consistent with the Green's function interpretation of the kernel  $\mathcal{M}_G$  which yield coordinate independent scalars E/B. From Eq. (3.8) it is clear that  $\mathcal{M}_G$  can be interpreted in the following ways:

$$\begin{bmatrix} E = \text{Re}(\mathcal{M}_G) \\ B = \text{Im}(\mathcal{M}_G) \end{bmatrix} \leftarrow \begin{bmatrix} Q = \delta(\hat{n} - \hat{n}_q) \\ U = 0 \end{bmatrix} \quad ; \quad \begin{bmatrix} E = -\text{Im}(\mathcal{M}_G) \\ B = +\text{Re}(\mathcal{M}_G) \end{bmatrix} \leftarrow \begin{bmatrix} Q = 0 \\ U = \delta(\hat{n} - \hat{n}_q) \end{bmatrix} , \quad (3.15)$$

$\mathcal{M}_B^*$  is the Greens function of the operator that transforms E/B to Stokes parameters Q/U. The real and imaginary parts of  $\mathcal{M}_B^*$  are identical irrespective of the galactic longitude, however they vary as a function of galactic latitude. This latitude dependent shape is necessary as the coordinate dependence of the Stokes parameters derived from the scalar E/B is built in via this Greens function. From Eq. (3.13) it is clear that  $\mathcal{M}_B^*$  can be interpreted in the following manner:

$$\begin{bmatrix} Q = \text{Re}(\mathcal{M}_B^*) \\ U = \text{Im}(\mathcal{M}_B^*) \end{bmatrix} \leftarrow \begin{bmatrix} E = \delta(\hat{n} - \hat{n}_e) \\ B = 0 \end{bmatrix} \quad ; \quad \begin{bmatrix} Q = -\text{Im}(\mathcal{M}_B^*) \\ U = \text{Re}(\mathcal{M}_B^*) \end{bmatrix} \leftarrow \begin{bmatrix} E = 0 \\ B = \delta(\hat{n} - \hat{n}_e) \end{bmatrix} . \quad (3.16)$$

### 3.4 Purifying Stokes parameters Q/U for E/B modes

We can only measure the total Stokes vector, a sum of the part corresponding to scalar  $E$  and the part corresponding to  $B$ . The  $E/B$  modes are orthogonal to each other in the sense that their respective operators are orthogonal to each other as discussed in Sec. 2.3.

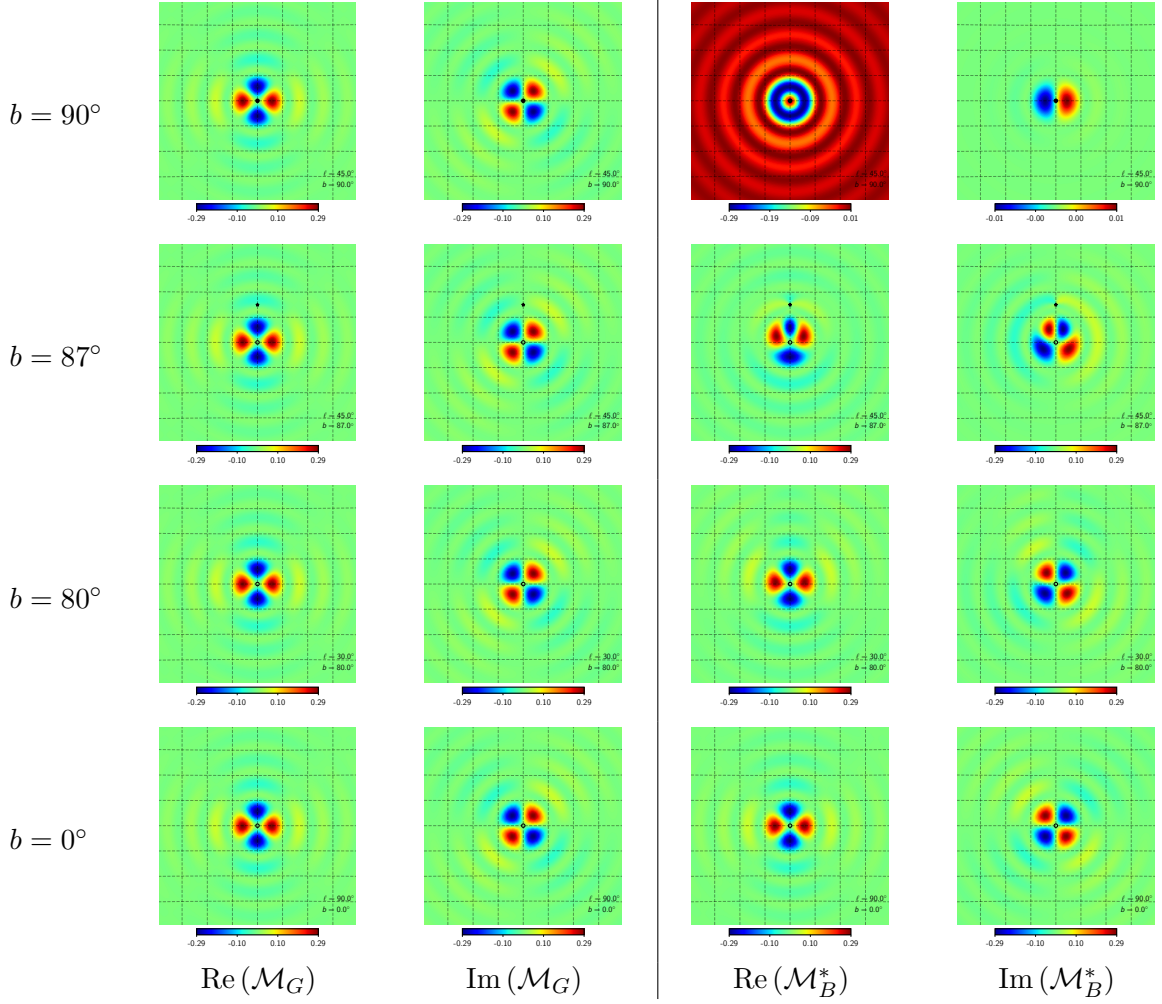


**Figure 3:** Real and imaginary parts of real space kernels for  $Q/U$  to  $E/B$  translation (and vice versa). The function  $\mathcal{M}_G$  is the Green's function (radiation kernel) that gives  $E + iB$  for a delta function Stokes input  ${}_{+2}X = Q + iU$  at the center. On the other hand,  $\mathcal{M}_B^*$  is the Green's function (radiation kernel) that gives  ${}_{+2}X$  for a delta function scalar input  $E + iB$  at the center. The black circles denotes the position of the center around which the kernels have been evaluated while the black star marks the location of the North Pole. The four rows depict the kernels at different latitudes on the sphere. The kernels are unchanged for center points at constant latitude.  $\mathcal{M}_G$  is invariant over the sphere because  $E/B$  fields are coordinate independent. In the convolution kernels,  $\mathcal{M}_G$  and  $\mathcal{M}_B$  switch roles. The kernels have been evaluated with the band limit  $\ell \in [2, 192]$  and sampled at the HEALPix resolution parameter  $\text{NSIDE}=2048$ . Each panel is approximately  $16^\circ \times 16^\circ$  in size with grid lines every 2 degrees.

It is possible to decompose the Stokes vector  $\bar{P}$  into one  $\bar{P}_E$  that purely contributes to  $E$  modes and another  $\bar{P}_B$  that purely contribute to the  $B$  modes of polarization. In this section we derive the real space operators which operate on the total Stokes vector and yield this decomposition, without ever having to explicitly evaluate the scalar modes. The algebra

is more involved, but the derivation is similar to that discussed in Sec. 3.1, so we refrain from presenting the detailed calculations here, and outline only the key points. We use the harmonic space projection operators  $\tilde{O}_{E/B}$ , defined in Eq. (2.13), to derive the respective real space operators. The Stokes parameters corresponding to each scalar mode are given by the following expressions:

$$\begin{aligned}\bar{P}_E &= [\bar{T}^{-1} {}_2\mathcal{Y} \tilde{T} \tilde{O}_E \tilde{T}^{-1} * {}_2\mathcal{Y}^\dagger \bar{T}] \bar{P}, \\ &= [\frac{1}{4} \bar{T}^\dagger {}_2\mathcal{Y} \tilde{T} \tilde{O}_E \tilde{T}^\dagger {}_2\mathcal{Y}^\dagger \bar{T}] \bar{P}, \\ &= \bar{O}_E \bar{P},\end{aligned}\tag{3.17}$$

$$\begin{aligned}\bar{P}_B &= [\bar{T}^{-1} {}_2\mathcal{Y} \tilde{T} \tilde{O}_B \tilde{T}^{-1} {}_2\mathcal{Y}^\dagger \bar{T}] \bar{P}, \\ &= [\frac{1}{4} \bar{T}^\dagger {}_2\mathcal{Y} \tilde{T} \tilde{O}_B \tilde{T}^\dagger {}_2\mathcal{Y}^\dagger \bar{T}] \bar{P}, \\ &= \bar{O}_B \bar{P}.\end{aligned}\tag{3.18}$$

We contract over all the matrix operators to arrive at the the real space operators. On working through the algebra it can be shown that the real space operators have the following form:

$$\bar{O}_{E/B} = 0.5\Delta\Omega \left\{ \begin{bmatrix} \mathcal{I}_r & \mathcal{I}_i \\ -\mathcal{I}_i & \mathcal{I}_r \end{bmatrix} \pm \begin{bmatrix} \mathcal{D}_r & \mathcal{D}_i \\ \mathcal{D}_i & -\mathcal{D}_r \end{bmatrix} \right\},\tag{3.19}$$

where  $\mathcal{I}_r$  &  $\mathcal{D}_r$  and  $\mathcal{I}_i$  &  $\mathcal{D}_i$  are the real and complex parts of the following complex functions:

$$\mathcal{I}(\hat{n}_e, \hat{n}_q) = \mathcal{I}_r + i\mathcal{I}_i = \sum_{\ell m} {}_2Y_{\ell m}(\hat{n}_e) {}_2Y_{\ell m}^*(\hat{n}_q),\tag{3.20a}$$

$$\mathcal{D}(\hat{n}_e, \hat{n}_q) = \mathcal{D}_r + i\mathcal{D}_i = \sum_{\ell m} {}_2Y_{\ell m}(\hat{n}_e) {}_2Y_{\ell m}^*(\hat{n}_q).\tag{3.20b}$$

These functions can be further simplified using the identity of spin spherical harmonics given in Eq. (3.4). Specifically it can be shown that these functions reduce to the following mathematical forms:

$$\mathcal{I}(\hat{n}_e, \hat{n}_q) = \sum_{\ell} \sqrt{\frac{2\ell+1}{4\pi}} {}_2Y_{\ell 2}(\beta_{qe}, \alpha_{qe}) e^{i2\gamma_{qe}} = \mathcal{I}_r + i\mathcal{I}_i,\tag{3.21a}$$

$$\mathcal{I}_r + i\mathcal{I}_i = \left[ \cos(2\alpha_{qe} + 2\gamma_{qe}) + i \sin(2\alpha_{qe} + 2\gamma_{qe}) \right] \mathcal{I}f(\beta_{qe}, \ell_{\min}, \ell_{\max}),\tag{3.21b}$$

$$\mathcal{D}(\hat{n}_q, \hat{n}_e) = \sum_{\ell} \sqrt{\frac{2\ell+1}{4\pi}} {}_2Y_{\ell 2}(\beta_{qe}, \alpha_{qe}) e^{-i2\gamma_{qe}} = \mathcal{D}_r + i\mathcal{D}_i,\tag{3.22a}$$

$$\mathcal{D}_r + i\mathcal{D}_i = \left[ \cos(2\alpha_{qe} - 2\gamma_{qe}) + i \sin(2\alpha_{qe} - 2\gamma_{qe}) \right] \mathcal{D}f(\beta_{qe}, \ell_{\min}, \ell_{\max}),\tag{3.22b}$$

where the radial functions are given by:

$$\mathcal{D/I}f(\beta, \ell_{\min}, \ell_{\max}) = \sum_{\ell=\ell_{\min}}^{\ell_{\max}} \sqrt{\frac{2\ell+1}{4\pi}} \mathcal{D/I}f_{\ell}(\beta),\tag{3.23}$$

where the functions  ${}_{\mathcal{D}/\mathcal{I}}f_\ell(\beta)$  are expressed in terms of  $P_\ell^2$  Legendre polynomials and are given by the following explicit mathematical forms:

$$\begin{aligned} {}_{\mathcal{D}/\mathcal{I}}f_\ell(\beta) &= 2 \frac{(\ell-2)!}{(\ell+2)!} \sqrt{\frac{2\ell+1}{4\pi}} \left[ -P_\ell^2(\cos\beta) \left( \frac{\ell-4}{\sin^2\beta} + \frac{1}{2}\ell(\ell-1) \pm \frac{2(\ell-1)\cos\beta}{\sin^2\beta} \right) \right. \\ &\quad \left. + P_{\ell-1}^2(\cos\beta) \left( (\ell+2) \frac{\cos\beta}{\sin^2\beta} \pm \frac{2(\ell+2)}{\sin^2\beta} \right) \right]. \end{aligned} \quad (3.24)$$

Finally the Stokes parameters corresponding to the respective scalar fields can be computed by evaluating the following expressions:

$$\begin{aligned} \begin{bmatrix} Q_e \\ U_e \end{bmatrix}_{E/B} &= \sum_{q=1}^{N_{\text{pix}}} \left\{ \mathcal{I}f(\beta_{qe}, \ell_{\min}, \ell_{\max}) \begin{bmatrix} \cos(2\alpha_{qe} + 2\gamma_{qe}) & \sin(2\alpha_{qe} + 2\gamma_{qe}) \\ -\sin(2\alpha_{qe} + 2\gamma_{qe}) & \cos(2\alpha_{qe} + 2\gamma_{qe}) \end{bmatrix} \begin{bmatrix} Q_q \\ U_q \end{bmatrix} \right. \\ &\quad \left. \pm {}_{\mathcal{D}}f(\beta_{qe}, \ell_{\min}, \ell_{\max}) \begin{bmatrix} \cos(2\alpha_{qe} - 2\gamma_{qe}) & \sin(2\alpha_{qe} - 2\gamma_{qe}) \\ \sin(2\alpha_{qe} - 2\gamma_{qe}) & -\cos(2\alpha_{qe} - 2\gamma_{qe}) \end{bmatrix} \begin{bmatrix} Q_q \\ U_q \end{bmatrix} \right\} \frac{\Delta\Omega}{2}, \end{aligned} \quad (3.25)$$

where all the symbols have their usual meaning. The above expression can be cast in the further simplified form,

$$\begin{aligned} {}_{+2}X_{E/B}(\hat{n}_e) &= 0.5\Delta\Omega \sum_{q=1}^{N_{\text{pix}}} \mathcal{I}f(\beta_{qe}) e^{-i2(\alpha_{qe} + \gamma_{qe})} {}_{+2}X(\hat{n}_q) \pm {}_{\mathcal{D}}f(\beta_{qe}) e^{i2(\alpha_{qe} - \gamma_{qe})} {}_{+2}X(\hat{n}_q)^*, \\ &= 0.5 \left\{ {}_{+2}X \mathcal{I}_G \pm {}_{+2}X^* \mathcal{D}_G \right\} \quad \text{Radiation kernel}, \end{aligned} \quad (3.26a)$$

$$= 0.5 \left\{ \mathcal{I}_B \star {}_{+2}X \pm \mathcal{D}_B \star {}_{+2}X^* \right\} \quad \text{Convolution kernel}, \quad (3.26b)$$

where all the symbols have their usual meaning and the explicit multipole dependence of the real space operators has been suppressed for brevity. Note that when the operators are expressed in terms of the Euler angles  $(\alpha_{qe}, \beta_{qe}, \gamma_{qe})$  they can be interpreted as the Greens functions and we denote them by  $\mathcal{I}_G = \Delta\Omega \mathcal{I}^*$  and  $\mathcal{D}_G = \Delta\Omega \mathcal{D}$ . When expressed as function of Euler angles  $(\alpha_{eq}, \beta_{eq}, \gamma_{eq})$  corresponding to the inverse rotations they can be interpreted as some convolving beam and we denote them by  $\mathcal{I}_B = \Delta\Omega \mathcal{I}$  and  $\mathcal{D}_B = \Delta\Omega \mathcal{D}$ . Note that unlike in the case of the operators  $\mathcal{M}_G$  and  $\mathcal{M}_B$  which have different shapes owing to their dependence on Euler angles  $\alpha$  and  $\gamma$  respectively, the operators  $\mathcal{D}_G$  and  $\mathcal{D}_B$  are identical since  $(\alpha_{qe} - \gamma_{qe}) = (\alpha_{eq} - \gamma_{eq})$ , while  $\mathcal{I}_G$  and  $\mathcal{I}_B$  are related by conjugation since  $(\alpha_{qe} + \gamma_{qe}) = -(\alpha_{eq} + \gamma_{eq})$ .

The operator  $\mathcal{I}$  is Hermitian and is a band limited version of the delta function owing to the identity:  $\lim_{\ell \rightarrow \infty} \mathcal{I} = \delta(\hat{n}_i - \hat{n}_j)$ . For all practical purposes  $\mathcal{I}$  acts like an identity operator as ascertained by the following set of identities: (i)  $\mathcal{I}\mathcal{I} = \mathcal{I}$ ; (ii)  $\mathcal{D}\mathcal{I} = \mathcal{D}$ .  $\mathcal{D}$  is a complex but symmetric matrix and  $\mathcal{D}^*$  is its inverse in this band limited sense:  $\mathcal{D}^*\mathcal{D} = \mathcal{I}$ . Using these properties<sup>6</sup> of the operators  $\mathcal{I}$  and  $\mathcal{D}$ , one can verify that the real space operators

---

<sup>6</sup>While testing the real space operator identities one encounters terms like  $\mathcal{D}\mathcal{I}^*$ ,  $\mathcal{I}^*\mathcal{I}$  and  $\mathcal{I}\mathcal{I}^*$  which cannot be simply interpreted but they always occur in pairs with opposite signs that exactly cancel each other.

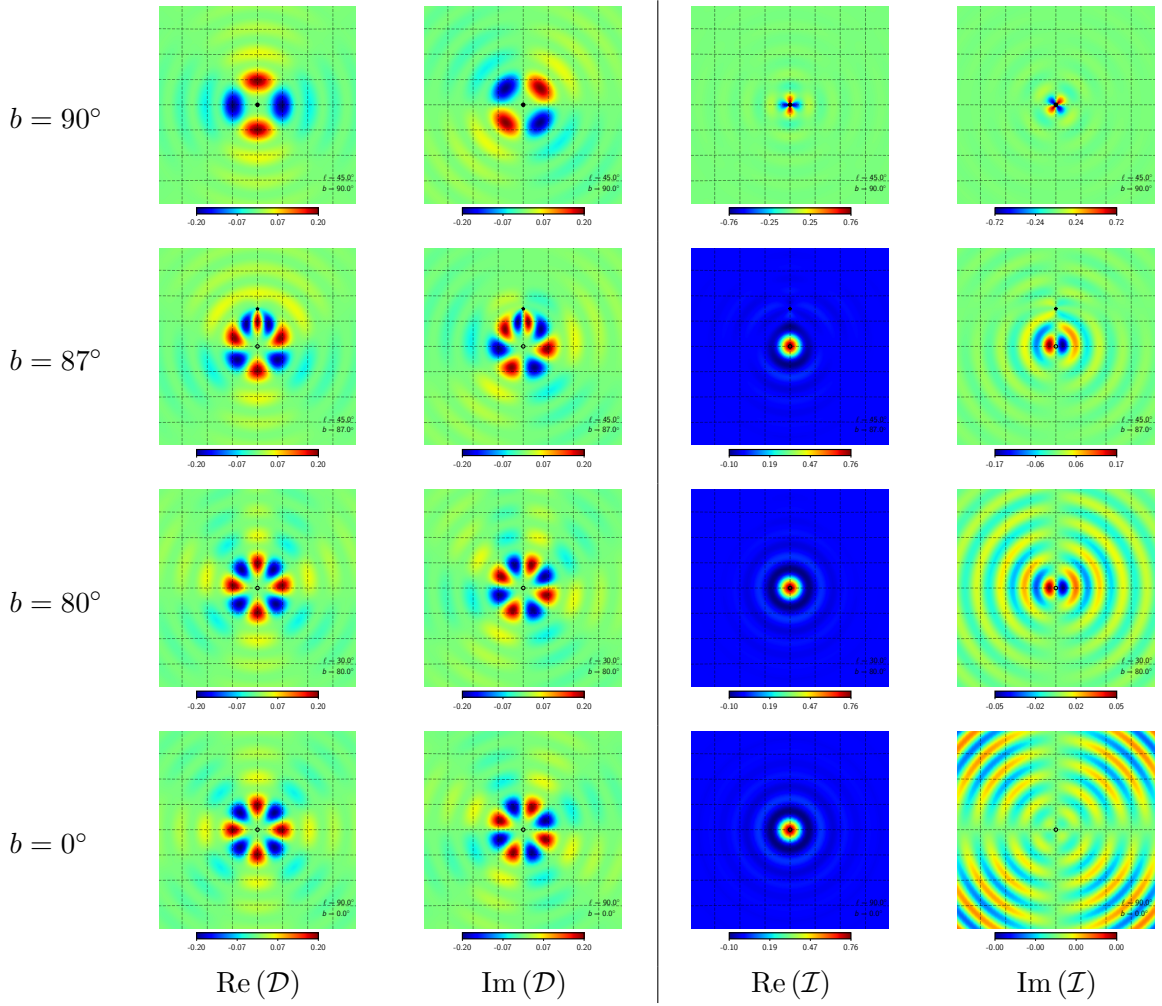


**Figure 4:** Like Figure 3, but for the kernels that purify Stokes parameter into their  $E/B$  parts.

satisfy the following identities:

$$\bar{\mathcal{O}}_E \bar{\mathcal{O}}_E = \bar{\mathcal{O}}_E \quad ; \quad \bar{\mathcal{O}}_B \bar{\mathcal{O}}_B = \bar{\mathcal{O}}_B , \quad (3.27a)$$

$$\bar{\mathcal{O}}_E \bar{\mathcal{O}}_B = 0 , \quad (3.27b)$$

$$\bar{\mathcal{O}}_E + \bar{\mathcal{O}}_B = \mathcal{I} , \quad (3.27c)$$

which are the real space analogues of their harmonic space counterparts discussed in Sec. 2.3. Thus they are exactly orthogonal and idempotent. Note that unlike in the harmonic case, the sum of the operators is the band limited identity operator  $\mathcal{I}$ . This non-exactness is representative of the loss of information resulting from making this transformation on measured data with some imposed band limit. Forcing the sum of the operators to be exactly an identity matrix compromises the orthogonality property of the  $\bar{\mathcal{O}}_E$  &  $\bar{\mathcal{O}}_B$  operators which is exact and a more crucial property of the operators.

The kernels  $\mathcal{D}$  &  $\mathcal{I}$  vary significantly as a function of galactic latitude of the central pixel as seen in Fig. 4. These kernels show a two fold symmetry in the vicinity of the poles

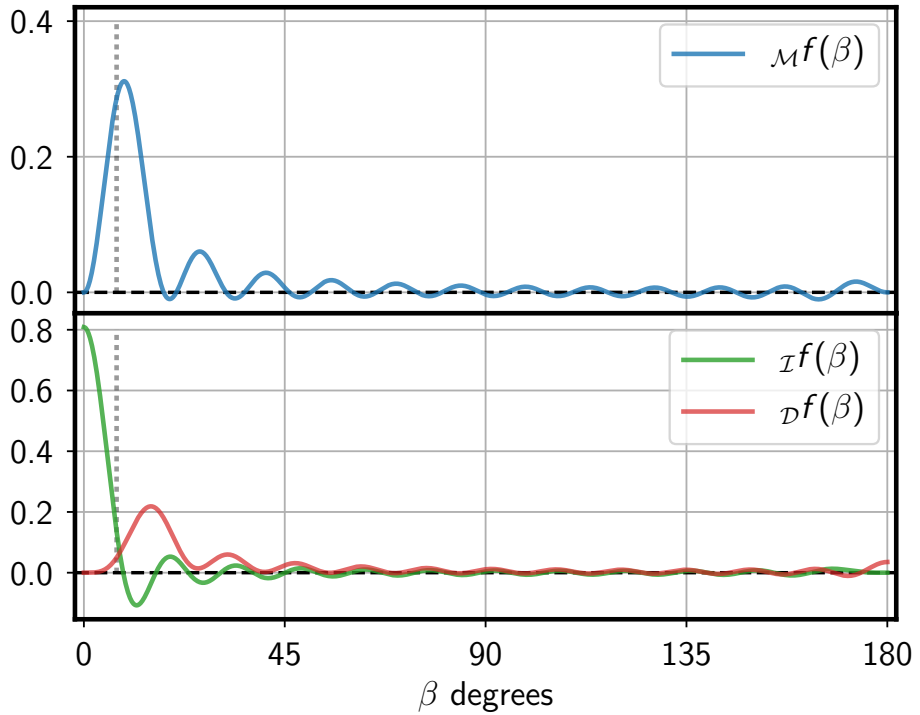


**Figure 5:** The figure depicts the radial part of the convolution kernels. These radial function have been evaluated with the band limit fixed at  $\ell \in [2, 24]$ . The vertical dashed line marks the approximate Healpix pixel size of a NSIDE=8, which is the lowest resolution that allows access to  $\ell_{\max} = 24$ .

and this arises due to Euler angle  $\gamma \approx 0$  here and therefore  $e^{i2(\alpha \pm \gamma)} \approx e^{i2\alpha}$ . Note that in this region, the azimuthal profile of the real and imaginary part of these kernels is identical to  $-\mathcal{M}_G$ . This explains why the imaginary part of the band limited delta function  $\mathcal{I}$  contributes just as much as the real part in these regions. On transiting to lower latitudes,  $\mathcal{D}$  quickly transitions to having a four fold symmetry while  $\mathcal{I}$  transitions to being dominated by the real part and behaves more like the conventional delta function. This transition can be most easily understood in the flat sky limit where  $\gamma \approx -\alpha$  which leads to the resultant 4 fold symmetry seen for  $\mathcal{D}$  owing to  $e^{i2(\alpha-\gamma)} \approx e^{i4\alpha}$  and  $\mathcal{I}$  being dominated by the real part owing to  $e^{-i2(\alpha+\gamma)} \approx 1 + i0$ . Since the flat sky approximation has most validity in the proximity of the equator these limiting tendencies of the respective kernels are seen in the bottom row of Fig. 4 which depict the kernels evaluated at the equator  $b = 0^\circ$ . The middle two row depict the kernels evaluated at intermediate latitudes:  $b = 87^\circ$  &  $80^\circ$  and serve to indicate the rate of this transition. These kernels are invariant under changes in longitude of the central pixel, the latitude being held fixed, as one may have expected.

### 3.5 The non-locality of the real space operators

We have explored in detail the azimuthal dependence of the real space kernels. Here we probe the radial dependence, which both determines the non-locality of the operators and encodes all their multipole dependencies. For illustration, Fig. 5 shows the radial kernels  $\mathcal{M}f$ ,  $\mathcal{D}f$ ,  $\mathcal{I}f$ , evaluated using the respective multipole sums given in Eq. (3.5b) and Eq. (3.23) in the band

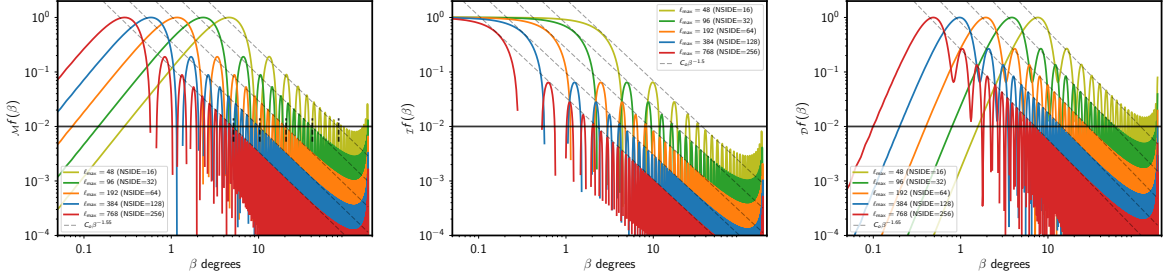


**Figure 6:** This figure depicts the radial functions for the different kernels and varying band limit set by fixed  $\ell_{\min} = 2$  and varying  $\ell_{\max}$  as indicated by their legends. The left panel depicts  $Mf(\beta, \ell_{\min}, \ell_{\max})$ , the middle panels depict  $xf(\beta, \ell_{\min}, \ell_{\max})$  and the right panel depicts  $Df(\beta, \ell_{\min}, \ell_{\max})$  respectively. All the curves are normalized such that their maxima is set to unity. The horizontal solid black line marks the location where the amplitude of the respective kernels fall below 1% of its maximum. The thin slanted dashed gray lines indicate a power law fit (by eye) to the envelope of the radial functions. The thick black short vertical dashed lines indicate the transition points as predicted by the empirically derived relation for the non-locality parameter  $\beta_0 = \min(180, 180 \frac{22}{\ell_{\max}})$ .

limit  $\ell \in [2, 24]$ . We choose a low band limit to evaluate these radial kernels to highlight some key features of their radial profile.

The function  $Mf$  is the radial part of the kernel that translates the Stokes parameters  $Q/U$  to scalars  $E/B$  and vice versa. As a consequence of the spin-2 symmetry, it vanishes as  $\beta \rightarrow 0$  and  $\beta \rightarrow \pi$ , since the Euler angles  $\alpha, \gamma$  are not uniquely defined at separations  $\beta = 0, \pi$ .

The radial part of the kernel that decomposes the Stokes parameters into parts that correspond to E and B modes are also necessarily non-local. The function  $xf$  is the radial part of the band limited delta function  $\mathcal{I}$ . It expectedly has its maxima at  $\beta = 0$  and decays with increasing angular separation.  $Df$  has a vanishing value in the region where  $\beta \rightarrow 0$  however it does not vanish at  $\beta \rightarrow \pi$  as seen in Fig. 5.

**Band limit dependence.** To quantify this non-locality, we study the radial extent of the kernels and its dependence on the maximum multipole accessible. We evaluate the radial functions for different values of  $\ell_{\max}$ , while keeping the lowest multipole fixed at  $\ell_{\min} = 2$ .

The resultant set of radial function are depicted in Fig. 6. While the amplitude of these radial function scales up as  $\propto \ell_{\max}^2$ , this feature of the kernels has been suppressed as all the function have been normalized such that their global maxima is set to unity. This normalization highlights the key feature, that on increasing  $\ell_{\max}$  the radial kernels shift left, attaining their global maxima at progressively small angular distances  $\beta$ . At intermediate values of  $\beta$ , the envelope of the radial functions is fit well by a power law  $\propto \beta^{-n}$  as seen in Fig. 6. In fact these finding are neatly summarized in the observation that the radial functions computed by evaluating the multipole sums to different maximum multipoles are self similar and follow this interesting telescoping and scaling property:

$$rf(\beta, 2, \ell_{\max}) \approx \left[ \frac{\ell_{\max}}{\ell'_{\max}} \right]^2 rf(\beta' = \frac{\ell'_{\max}}{\ell_{\max}} \beta, 2, \ell'_{\max}),$$

where  $rf$  denotes all the different radial functions.

We can now understand the shifting left of the radial kernels on increasing the maximum multipole using this telescoping property. Lets say the function  ${}_rf(\beta', \ell'_{\max})$  transition to being monotonously below some fraction of the global maxima at an angular distance of  $\beta'_0$ . The function  ${}_rf(\beta, \ell_{\max})$ , given  $\ell_{\max} > \ell'_{\max}$ , reaches the same transition point at a smaller angular distance  $\beta$ . The amplitude scaling of the functions is irrelevant since the transition point is always described in terms of the fraction of the global maxima of the function.

To quantify the non-locality of the scalar modes  $E/B$ , we can define a characteristic angular radius of the region from which the kernels get most of their contribution. We define a non-locality parameter  $\beta_0$  as the angle beyond which the function  ${}_Mf(\beta, \ell_{\min} = 2, \ell_{\max})$  consistently falls below 1% of its maximum. The empirical relation:

$$\beta_0 = \min \left( 180, 180 \frac{\ell_0}{\ell_{\max}} \right), \quad (3.28)$$

with  $\ell_0 = 22$  provides a reasonable estimate of this transition point for  ${}_Mf$  as seen in Fig. 6. Setting  $\ell_0 = 10$  and  $\ell_0 = 32$  predicts the transition points for the functions  ${}_Tf$  and  ${}_Df$  respectively.  $\Rightarrow$  How sensitive is this transition point to  $\ell_{\min}$ ?

$\Rightarrow$  Compare the fitted slope to the one in the Zaldariaga paper.

### 3.6 Generalized polarization operators

With our better understanding of the radial part of the kernel for CMB polarization, we can write down generalized  $E/B$ -like fields that depend on a different radial function, even one that we specify to have compact support. The spin symmetry constrains the azimuthal part of the real space kernels to be of the form  $\sim e^{\pm i2\alpha}$ . The shape of the radial part of the operator is determined by the basis functions and varies as a function of the band limit. It is here that we may potentially choose alternate forms for the radial functions to suit certain kind of analysis.

We can systematically generalize the real space operator by introducing the following harmonic space filter function:

$$\tilde{\mathcal{G}} = \begin{bmatrix} g_\ell^E & 0 \\ 0 & g_\ell^B \end{bmatrix}, \quad (3.29)$$

where the functions  $g_\ell^E$  and  $g_\ell^B$  represent the harmonic representation of the modified radial functions and can in the most general case be chosen to be different for  $E$  and  $B$  modes. To simplify discussions, we proceed by setting  $g_\ell^E = g_\ell^B = g_\ell$ . Given this harmonic function  $g_\ell$ , we can define the real space operator  $\bar{O}'$  which translates Stokes  $Q/U$  to scalars  $E/B$  and the inverse operator  $\bar{O}'^{-1}$  in the following manner,

$$\bar{O}' = {}_0\mathcal{Y}\tilde{T}^{-1}\tilde{\mathcal{G}}_2\mathcal{Y}^\dagger\bar{T}, \quad (3.30a)$$

$$\bar{O}'^{-1} = \bar{T}^{-1}{}_2\mathcal{Y}\tilde{\mathcal{G}}^{-1}\tilde{T}_0\mathcal{Y}^\dagger. \quad (3.30b)$$

The primed notation distinguishes these generalized operators from the default operators defined in Sec. 3.1 and Sec. 3.2. We require both the forward and inverse operators to be well defined. This constrains the choice of  $\tilde{\mathcal{G}}$  to have a valid inverse and is important to recover the standard CMB power spectra. The radial parts of this generalized operator and

its inverse are given by the following expressions,

$$G_{QU \rightarrow EB}(\beta) = G(\beta) = \sum_{\ell=2}^{\ell_{\max}} g_\ell \frac{2\ell+1}{4\pi} \sqrt{\frac{(\ell-2)!}{(\ell+2)!}} P_\ell^2(\cos \beta), \quad (3.31a)$$

$$G_{EB \rightarrow QU}(\beta) = G^{-1}(\beta) = \sum_{\ell=2}^{\ell_{\max}} g_\ell^{-1} \frac{2\ell+1}{4\pi} \sqrt{\frac{(\ell-2)!}{(\ell+2)!}} P_\ell^2(\cos \beta). \quad (3.31b)$$

The default radial function is just a special case resulting from the choice  $\tilde{\mathcal{G}} = \mathbb{1}$  ( $g_\ell = 1$ ), in which case  $\tilde{\mathcal{G}}^{-1} = \tilde{\mathcal{G}}$  and therefore  $G^{-1}(\beta) = G(\beta) = \mathcal{M}f$ .

While defining these generalized operators, it is more natural to choose the real space function  $G(\beta)$  rather than the harmonic space  $g_\ell$ , bearing in mind the constraint that  $G(\beta = 0) = G(\beta = \pi) = 0$ . Employing the orthogonality property of associated Legendre polynomials it can be shown that the harmonic function  $g_\ell$  is given by the expression,

$$g_\ell = 2\pi \sqrt{\frac{(\ell-2)!}{(\ell+2)!}} \int_0^\pi G(\beta) P_\ell^2(\cos \beta) d\cos \beta. \quad (3.32)$$

An arbitrary  $G(\beta)$  for which  $g_\ell \neq 1$  can be equivalently thought in terms of the standard  $E/B$  fields being convolved with some effective circularly symmetric beam whose radial profile is given by the expression,

$$b(\beta) = \sum_{\ell=0}^{\ell_{\max}} \frac{2\ell+1}{4\pi} g_\ell P_\ell^0(\cos \beta), \quad (3.33)$$

where  $g_\ell$  is the same harmonic function as that appearing in Eq. (3.31). In contrast to the radial function  $G(\beta)$  an instrumental beam function appropriately normalized has the property  $b(\beta) \rightarrow 1$  as  $\beta \rightarrow 0$ . Though the real space behavior of these two function  $G(\beta)$  and  $b(\beta)$  has these differences, in harmonic space they play identical roles.

In Fig. 7, we examine in more detail the relationship between the modified radial kernels and these beam harmonic coefficients. Fig. 7(iii) depicts the radial profile of the effective beams corresponding to different radial kernels: the standard kernel with a radial cutoff, kernels corresponding to Gaussian smoothings of the  $E/B$  fields, an radial function without oscillations and an exponential cutoff. Note that the smoothing tend to increase the non-locality, indicated by the shifting right of the maxima of the respective kernels, as one may have expected. The exponential cutoff (red curve) by construction has a very small non-locality (parameterized by  $\beta_0$ ).

Fig. 7(ii) depicts the harmonic description  $g_\ell$  for these respective radial kernels and beams. Finally, the beam that the modified radial kernels applies to the  $E/B$  fields we show in Fig. 7(iii). Note that the beam function corresponding to the default radial kernel ( $g_\ell = 1$ ) is merely a band limited representation of a delta-function beam.

### 3.6.1 Recovering the standard $E$ and $B$ mode spectra

The generalized convolution kernels defined in the previous section, when operated on the Stokes vector returns some scalar  $E'$  and  $B'$  mode maps,

$$\bar{S}' = \bar{O}' \bar{P} \quad (3.34)$$

which are merely filtered versions of the standard  $E/B$  modes maps. Since the filter function is simply  $g_\ell$ , easily obtained from the modified radial function  $G(\beta)$ , and it can be simply

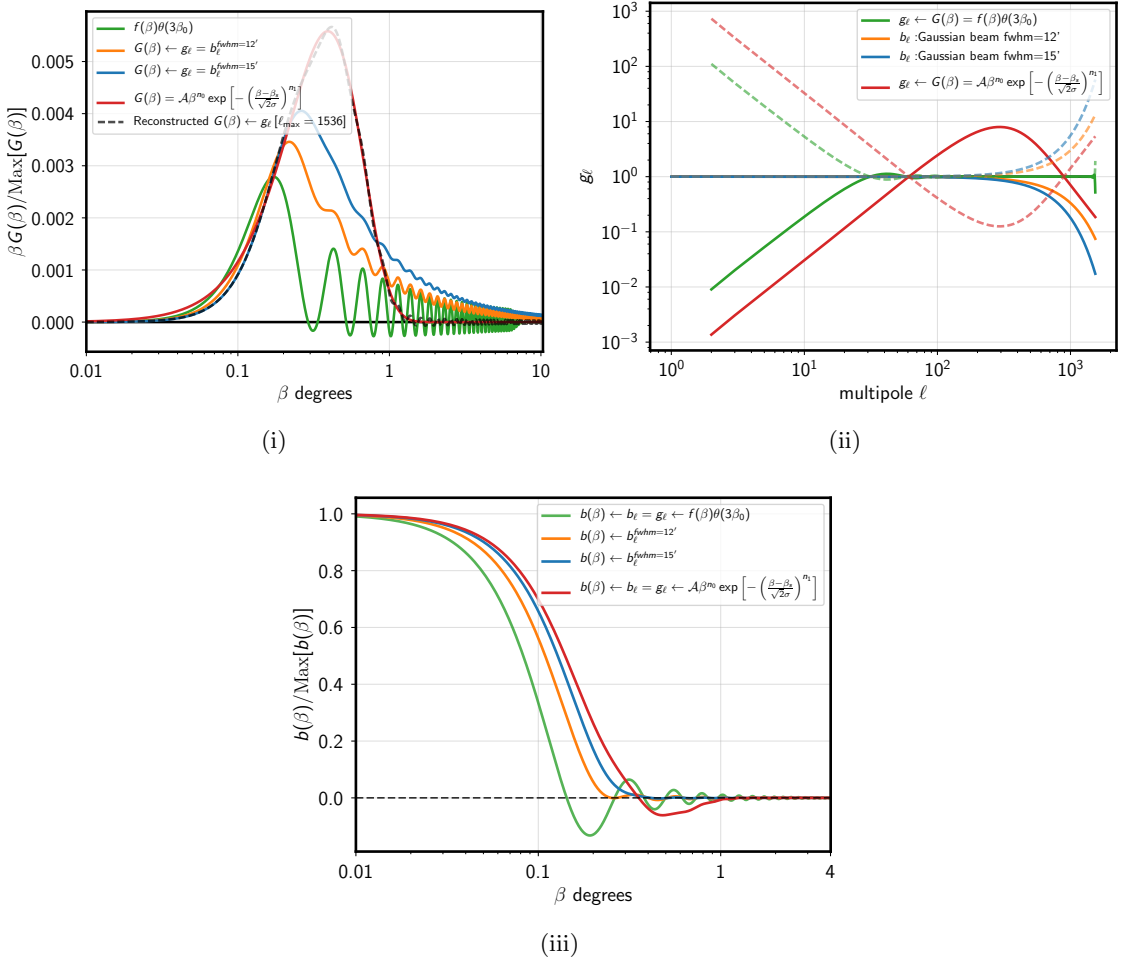


**Figure 7:** *Top left:* The green line depicts the default radial kernel  $f(\beta)$  defined in Eq. (3.5), multiplied by an apodized step function  $\theta(3\beta_0)$ . The blue and orange lines depict the modified radial function resulting in the beam harmonics  $b_\ell$  corresponding to Gaussian beams with fwhm=15 & 12 arc-minutes respectively. The red curve depicts an example modified radial function:  $G(\beta) = A\beta^{n_0} \exp\left[-\left(\frac{\beta-\beta_s}{\sqrt{2}\sigma}\right)^{n_1}\right]$  with parameters set to the following values [ $n_0 = 1; \beta_s = 0; \sigma = 0.004; n_1 = 1.5$ ]. The black dashed curve depicts the band limited reconstruction of the modified radial function. *Top right:* This figure depicts the harmonic representation of the respective radial functions as indicated by the legend. The dashed curves of the corresponding color depict the inverse of the harmonic functions. *Bottom:* This figure depicts the normalized beam function  $b(\beta)$  evaluated from interpreting the respective harmonic functions as those corresponding to an effective instrument beam.

interpreted as the harmonic coefficients of some azimuthally symmetric beam, the power spectra of the modified scalar fields  $E'$  and  $B'$  are related to the spectra of the standard  $E$  and  $B$  fields via the following relation,

$$C_\ell^{EE, BB, EB} = C_\ell^{E'E', B'B', E'B'} / g_\ell^2, \quad (3.35a)$$

$$C_\ell^{TE, TB} = C_\ell^{TE', TB'} / g_\ell, \quad (3.35b)$$

where  $C_\ell$  denotes the angular power spectra and  $T$  refers to the temperature anisotropy map. Therefore the standard CMB spectra can always be recovered as long as the  $1/g_\ell$  and  $1/g_\ell^2$  are well behaved functions, which can be ensured by making a suitable choice for the modified radial function  $G(\beta)$ .

### 3.6.2 Relation to the spin raising $\bar{\partial}^2$ and lowering $\bar{\partial}^2$ operators

Recall that on operating twice with the spin lowering operator on the Stokes charge  $+_2X$  results in filtered version of  $E/B$  maps as in Eq. (2.4). Now note that it is possible to construct a modified real space operator by choosing the harmonic space function to be  $g_\ell = \sqrt{\frac{(\ell+2)!}{(\ell-2)!}}$ , resulting in similarly filtered  $E/B$  maps as follows:

$$[\mathcal{E} + i\mathcal{B}](\hat{n}_e) = -\Delta\Omega \sum_{q=1}^{N_{\text{pix}}} \left\{ \left[ \sum_{\ell=\ell_{\min}}^{\ell_{\max}} \frac{2\ell+1}{4\pi} P_\ell^2(\beta_{qe}) \right] e^{-i2\alpha_{eq}} {}_2X(\hat{n}_q) \right\}. \quad (3.36)$$

Comparing Eq. (2.4a) to Eq. (??) makes apparent the following mapping:

$$\bar{\partial}^2 \equiv \Delta\Omega \sum_{q=1}^{N_{\text{pix}}} \left[ \sum_{\ell=\ell_{\min}}^{\ell_{\max}} \frac{2\ell+1}{4\pi} P_\ell^2(\beta_{qe}) \right] e^{-i2\alpha_{eq}}. \quad (3.37)$$

The operator  $\bar{\partial}^2$  is composed of derivative operations and hence has an implicit bi-positional dependence for all numerical purposes which is made explicit in the band limited version of the operator. The band limited version of the spin raising operator  $\bar{\partial}^2$  is derived by merely taking the conjugate of the above equation.

## 4 Understanding polarization signatures of magnetized filaments

The real space kernels give us a better intuitive understanding of the  $E/B$  modes associated with physical objects. For example, a simple model for a magnetized filament has the magnetic field threaded along a linear gas overdensity. Precession of the dust grains around the magnetic field leads to a net polarization perpendicular to the magnetic field (and perpendicular to the filament overall). For a filament aligned North–South, the polarization will be horizontal or  $Q < 0$ ,  $U = 0$  (left pane of Fig. 8). The Green’s function kernels for horizontal polarization are rotated by 90 degrees relative to the components of  $\mathcal{M}_G$  in Fig. 3.

The kernel can be thought of as the orientable nib of a calligraphy pen or paintbrush that we can trace along the filament. The positive components for the  $E$  part of the Green’s function align and reinforce along the filament, and so the filament is highlighted as a segment with  $E > 0$ . Since the overdensity will also have emission in total intensity, this naturally predicts a positive  $TE$  correlation for magnetized filaments. The  $E$  pattern is somewhat negative along the outside of the filament, also a consequence of the kernel shape.

The  $B$  part of the Green’s function, traced along the filament, cancels itself except at the filament ends. This results in a non-zero  $B$  pattern for the filament. For a North–South filament, the  $B$ -mode pattern is positive on the North-East and South-West, and negative in the North-West and South-East.

The non-zero  $B$  result is somewhat surprising given that the polarization pattern is symmetric to both horizontal and vertical reflections through the filament center. However, unlike a circular ring, this filament is not a configuration with a definite parity. Because the

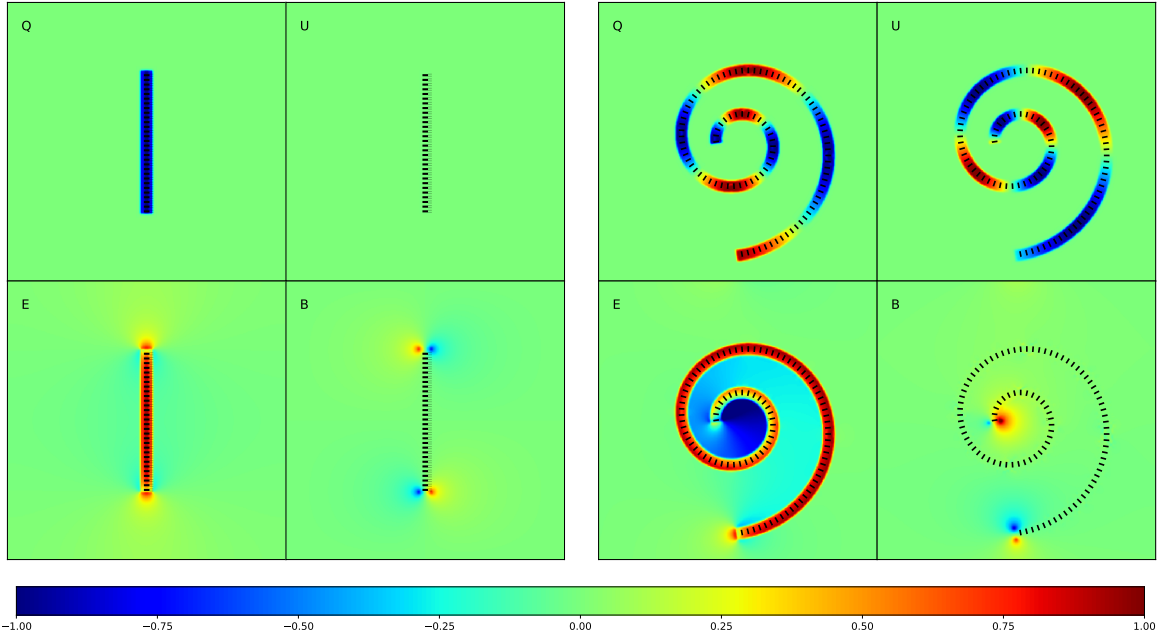


**Figure 8:** The polarization signals of toy filament structures. In a filament organized perfectly along a magnetic field line, the polarization will be perpendicular to the filament direction. The  $E/B$  modes of filaments are in some ways easier to think about than the Stokes parameters. Left panels: in a straight filament, the  $E$ -mode is positive along the filament and at the ends, but negative along the sides.  $B$ -modes are only non-zero at the ends. Right panels: in a curved filament, the  $E$ -mode is again positive along the filament. Outside the filament, the  $E$ -mode is more negative on the interior of the curve than the exterior. The  $B$ -modes are again non-zero only at the ends, and are akin to the straight filament case. In all images, the longitude angle increases to the left (East in sky convention). All plots are on a common, arbitrary color scale.

scalar polarization descriptions are coordinate independent, the  $E/B$  patterns do not depend on the orientation of the filament. A filament inclined at  $45^\circ$  will have a similar  $E/B$  pattern, but different reflection symmetries.

A stacking analysis of Planck data [15] sees  $E > 0$  along filaments (selected from intensity data), but claim no  $B$ -mode signal. We predict that a  $B$ -mode signal from filaments should be present. A naive filament stacking analysis is only suited for making  $E$ -mode detections. Detecting  $B$ -modes from filaments requires a more careful edge stacked filaments analysis. While the detectability of  $B$ -mode signature from filaments from Planck data calls for a more careful assessment, it should definitely be detectable in higher fidelity data.

The intuition from the real-space kernels holds also when we distort the shape of the filament. If the filament were bent around into a circle, the positive and negative parts of the  $B$  pattern will cancel, and we are left with a hoop of pure  $E$  pattern (note that this cancellation would not happen for an ellipse or any loop of non-constant radius of curvature). The same general description holds for a spiral-shaped filament, which can be viewed as distortion of the straight filament. The filament is highlighted by positive  $E > 0$ . The  $E$ -pattern is more negative on the interior of a curve than on the exterior, and the concentric rings of filamentary structure make an increasingly negative  $E$  value inside. The  $B$ -pattern

is again concentrated at the ends of the filament in an oriented pair of positive/negative fluctuations.  $\Rightarrow$  Add that the spiral has a constant radius of curvature and thats the reason you dont see B-mode signal in intermediate regions of the spiral!

Note that we have made the simplifying assumption that the polarization headless vectors are perpendicular to the tangent to the filament at any given point and this results in dominantly generating an E-mode signal while the B-mode signal is present only near the edges. By similar arguments it can be seen that that polarization pattern will be dominated by B-modes if the polarization vector is always at  $+45$  (or  $-45$ ) degrees to the tangent to the filament while the E-mode signal would only be present at the edges. Therefore a careful study of the  $E/B$  mode power in a filament can provide insights into the orientation of the magnetic field with respect to the length of the filament, assuming the polarization vectors (headless) are always perpendicular to the magnetic field vector.

## 5 Discussion

We introduced a vector-matrix notation which allows for concise book keeping of all the standard operations involved in the analysis of CMB polarization maps. This notation simplifies the derivation of the real space operators. We presented a first derivation of the real space operators on the sphere that transforms the Stokes vector  $\bar{P}$  to into a vector of scalars  $\bar{S}$  and vice versa. We also presented real space operators that directly decompose the full Stokes vector  $\bar{P}$  into vector  $\bar{P}_E$  and  $\bar{P}_B$  that correspond to the respective scalar modes.

These real space operators provide a spatially intuitive way of understanding the different decompositions of the Stokes vector. We explicitly demonstrated that all the real space operators have the common characteristic of being separable into a azimuthal part that is band limit independent and radial part that incorporates all the band limit dependence. The azimuthal part of the operator is primarily responsible for the requisite spinorial decomposition, while the radial weights determine the non-local dependence of the construction of the resultant fields on the original fields. Using the self similarity property of the radial functions we define a non-locality parameter and argued that it is proportional to  $\ell_{\max}^{-1}$ . The scalar decomposition of the Stokes parameters being of primary interest, we empirically derived the non-locality parameter  $\beta_0$  for this operation and showed that the proportionality constant  $\ell_0 = 22$  provided a good prediction for the angular distance at which the  $Mf$  falls below 1% of its maxima as seen in Fig. 6.

Our careful study of the real space operators reveals the dual interpretation of the operators as either the Green's function or a convolving beam depending on whether the kernels are expressed in terms of the forward rotation Euler angles or the inverse rotation Euler angles. While the convolution interpretation is a familiar one, the Green's function interpretation is a new way of looking at this operation. This new interpretation allows us to think of  ${}_{+2}X$  as some spin-2 charge which radiates out a complex spin-0 scalar field  $E + iB$ . The resultant complex scalar maps can be then understood as arising from superposition of the radiating field emanating from all the spin charges on the sphere. The  $E/B$  mode maps are merely the real and imaginary parts of this resultant complex scalar field.

A similar equation for real space  $E$  &  $B$  operators was derived in [11], however those results were derived for the flat sky case and did not explicitly derive the radial kernel.  $\Rightarrow$  A discussion on this should be in the conclusions.

Understanding the non-locality of the real space operators, allowed us to generalize the real space operators  $\bar{O}'$  and its inverse  $\bar{O}'^{-1}$ , which transform between the spin-2 and

spin-0 representations of the CMB polarization. We presented a method of systematically generalizing these operators by introducing the harmonic space operator  $\tilde{\mathcal{G}}$  which in effect causes the radial function to vary from its default form. We show that these modifications to the radial kernel can be interpreted as a smoothing operation on the scalar fields with a circularly symmetric instrument beam. We argue that one can choose any arbitrary form for  $\tilde{\mathcal{G}}$  as long as one adheres to the constraint that  $\tilde{\mathcal{G}}^{-1}$  and  $\tilde{\mathcal{G}}^{-2}$  are well defined operators. These constraints are necessary to ensure that all the standard CMB spectra are recoverable from the modified  $E'/B'$  maps emerging from the modified operators on the Stokes parameter maps. Noting that the standard spin raising  $\eth^2$  and spin lowering  $\bar{\eth}^2$  operators are special cases of these generalized operators, we presented a band limited representation of these operators.

Discussion on results from polarized filaments filaments, compare and contrast with those in [11].

There are several advantages and alternative analysis routes that emerge from employing these real space operators for analysis of CMB polarization maps. To begin with, one does not need to evaluate the spin harmonic functions as the real space operators only rely on computing the Euler angles which can be done on the fly and the  $P_\ell^2$  functions need to be tabulated only once for analysis at some predetermined resolution. Note that this real space analysis method trivially generalizes to analyzing maps of arbitrary spin. Especially given the Green's function interpretation of these operators, their implementation is trivially parallelizable, since the  $E/B$  contribution from the Stokes charge in each pixel can be evaluated independently. Also note that the evaluation of contribution from charges in the masked portion of the sky can be easily omitted, unlike in the harmonic analysis. Given the Green's function interpretation of the real space operators and their locality, suggests the possibility of converting the Stokes parameter time ordered data to scalar  $E/B$  time ordered data given the pointing model for the observations, which can then be subsequently converted to maps of  $E/B$  modes using standard map making techniques. Since the real space operators offer the ability of tuning the locality of  $E/B$  maps, this can be potentially exploited to reduce foreground contamination from distant parts of the sky. For instance the real space operators can be defined such that the locality of their radial kernels is varied on different portions of the sky, dictated by say the foreground morphology, resulting in some scalar  $E'/B'$  maps. While this idea seems promising, the usefulness of this implementation will depend on whether the standard  $E/B$  mode spectra are recoverable from scalar maps derived in this fashion. Note that it would be fairly non-trivial to think of such implementations using conventional harmonic space methods.

Results demonstrating the equivalence of these real space methods to the conventional harmonic space methods and from explorations of some of the ideas discussed above will be presented in the second part of this series of papers.

## Acknowledgments

This work was supported by NASA Astrophysics Theory Program under grant NNX17AF87G. We thank David C. Collins for useful discussions.

## References

- [1] W. Hu and M. White, *A CMB polarization primer*, *New Astronomy* **2** (Oct., 1997) 323–344, [[astro-ph/9706147](#)].

- [2] W. Hu and M. White, *CMB anisotropies: Total angular momentum method*, *Phys. Rev. D* **56** (July, 1997) 596–615, [[astro-ph/9702170](#)].
- [3] U. Seljak and M. Zaldarriaga, *Signature of Gravity Waves in the Polarization of the Microwave Background*, *Physical Review Letters* **78** (Mar., 1997) 2054–2057, [[astro-ph/9609169](#)].
- [4] Planck Collaboration, R. Adam, P. A. R. Ade, N. Aghanim, M. Arnaud, J. Aumont et al., *Planck intermediate results. XXX. The angular power spectrum of polarized dust emission at intermediate and high Galactic latitudes*, *A&A* **586** (Feb., 2016) A133, [[1409.5738](#)].
- [5] A. Kosowsky and A. Loeb, *Faraday Rotation of Microwave Background Polarization by a Primordial Magnetic Field*, *ApJ* **469** (Sept., 1996) 1, [[astro-ph/9601055](#)].
- [6] A. Lue, L. Wang and M. Kamionkowski, *Cosmological Signature of New Parity-Violating Interactions*, *Physical Review Letters* **83** (Aug., 1999) 1506–1509, [[astro-ph/9812088](#)].
- [7] L. Campanelli, A. D. Dolgov, M. Giannotti and F. L. Villante, *Faraday Rotation of the Cosmic Microwave Background Polarization and Primordial Magnetic Field Properties*, *ApJ* **616** (Nov., 2004) 1–7, [[astro-ph/0405420](#)].
- [8] L. Pogosian, *Searching for primordial magnetism with multifrequency cosmic microwave background experiments*, *MNRAS* **438** (Mar., 2014) 2508–2512, [[1311.2926](#)].
- [9] M. Kamionkowski, A. Kosowsky and A. Stebbins, *Statistics of cosmic microwave background polarization*, *Phys. Rev. D* **55** (June, 1997) 7368–7388, [[astro-ph/9611125](#)].
- [10] M. Zaldarriaga and U. Seljak, *All-sky analysis of polarization in the microwave background*, *Phys. Rev. D* **55** (Feb., 1997) 1830–1840, [[astro-ph/9609170](#)].
- [11] M. Zaldarriaga, *The nature of the E-B decomposition of CMB polarization*, *Phys. Rev. D* **64** (jun, 2001) 103001, [[0106174](#)].
- [12] M. Zaldarriaga and U. Seljak, *All-sky analysis of polarization in the microwave background*, *Phys. Rev. D* **55** (feb, 1997) 1830–1840, [[astro-ph/9609170](#)].
- [13] D. A. Varshalovich, A. N. Moskalev and V. K. Khersonskii, *Quantum Theory of Angular Momentum* (World Scientific). World Scientific, 1988.
- [14] J. N. Goldberg, A. J. Macfarlane, E. T. Newman, F. Rohrlich and E. C. G. Sudarshan, *Spin-s Spherical Harmonics and  $\delta$* , *J. Math. Phys.* **8** (nov, 1967) 2155–2161.
- [15] Planck Collaboration, P. A. R. Ade, N. Aghanim, M. Arnaud, M. Ashdown, J. Aumont et al., *Planck intermediate results. XXXVIII. E- and B-modes of dust polarization from the magnetized filamentary structure of the interstellar medium*, *A&A* **586** (Feb., 2016) A141.